Interconversion of hydrated protons at the interface between liquid water and platinum

Interconversion of Hydrated Protons at the Interface between Liquid Water and Platinum

Peter S. Rice, Yu Mao, Chenxi Guo and P. Hu*

School of Chemistry and Chemical Engineering, The Queen's University of Belfast, Belfast BT9 5AG, N. Ireland

Email: p.hu@qub.ac.uk

Abstract: Hydrogen transfer is the fundamental step involved in electrochemistry, being involved in water splitting and the hydrogen evolution reaction (HER). However, the nature of this process at the solid-liquid interface has been little studied at the atomic level. In this work, we use *ab initio* molecular dynamics (AIMD) and umbrella sampling (US), giving us an accurate description of the dynamic processes associated with the solid-liquid environment. Based on this method, the free energy barriers were calculated at the H_2O/Pt(111) interface, and a multistep mechanism has been proposed. We find that proton transfer is dictated by the strength of the solid-liquid interaction and the configuration of water molecules above the reaction site. In particular, we show that the presence of surface adsorbed cations, which are confined to the interface above the top site position, act as vessels for enhanced hydrogen transfer to and from the surface. Our results could lead to significant mechanistic consequences for HER, water splitting and solid-liquid reactions in general.

(Keywords: DFT, Free Energy, Pt (111), Solid-Liquid)

Introduction

In recent years, a concerted global emphasis has been placed on developing renewable energy sources as alternatives to fossil fuels[1,2]. Significant developments within the field of electrochemistry have resulted in numerous technological advancements in fuel cells[3] and batteries[4], to name just a few. Great progress has also been made in surface science, regarding the structural characterization at solid-liquid interfaces, thanks to the development of several in-situ techniques[5]. In particular, improvements in atomic force microscopy techniques (AFM)[6,7] and the emergence of high pressure X-ray photoelectron spectroscopy[8] (HPXPS) have permitted an in-situ characterization which goes beyond the restrictions of the ultra-high vacuum (UHV) conditions, commonly encountered in surface science. However, due to proton transfer processes being extremely fast, features including the reaction kinetics, free energy

barriers and the atomistic structures of intermediates along the reaction pathway remain challenging, even for current spectroscopic techniques to detect[9,10,11,12,13].

Working closely with experimental findings, several theoretical methods, based mainly on periodic density functional theory (DFT) modelled on noble metal surfaces, have been developed [14]. However, the complications and computational expenditure involved in explicitly modelling the electrode-electrolyte interface are by no way trivial. In spite of this, an array of modelling approaches have been developed over the past decade. Many of which have gained significant attention, differing in how they treat the water layer. For the majority of studies, systems are either modelled with an explicit water layer[15,16,17,18,19,20] , or the utilization of more computationally affordable (implicit solvation) methods such as continuum solvation models based on the modified Poisson-Boltzmann equations[21,22,23] .

Despite their computational affordability, many models lack important thermodynamic constraints, while static DFT calculations are often sensitive to the configurations of water molecules. For instance, Schnur and Groß[24] highlighted that the interfacial potential can vary by 2 V depending on the water layer orientation. It is clear that many methods have proven to be unrealistic representations, as they often neglect the effects of thermal fluctuations and molecular motion exhibited by water under standard conditions[25,26,27,28].

Furthermore, it remains difficult to fully explore reaction mechanisms at solid-liquid interfaces leaving many questions unanswered; for example, how the free energy profiles of surface reactions are calculated or to what extent these reactions are influenced by the water structure. The transfer of hydrogen in the form of hydrated protons has been identified as the key step in many chemical and biological systems, making it of cross-disciplinary importance. In electrochemistry, hydrogen transfer is the fundamental elementary step that gives rise to the electro-current, as well as being involved in water splitting and the hydrogen evolution reaction

(HER). Here, the solvated protons exist in equilibrium with adsorbed hydrogen on the metal surface[29,30,31,32,33]:

$$H_3O^+ + e^- \rightleftharpoons H_{ads} + H_2O$$

To the best of our knowledge, a method for accurately calculating the free energy barriers of hydrogen transfer has yet been reported that encompasses the description of dynamic processes associated with solid-liquid interfaces.

In this work, we address the fundamental processes associated with the solid-liquid interface at the atomic level, using first principles calculations. We investigate the H_nO^x/Pt(111) (n= 2 or 3; x= 0 or +1) interface (Figure 1) to gain a greater insight into how the water layer diverges from the neutral case on addition of H. Platinum (Pt) was chosen as it exhibits a superior catalytic activity compared to other noble metals, making it an ideal model system. We do this by utilizing an *ab initio* molecular dynamics (AIMD) approach including explicit solvent molecules on the solid surface. AIMD ensures that we do not rely on empirical assumptions of the solvation process while giving an accurate depiction of chemical bonds formed on the surface.[34]

To this end, we propose a mechanism which indicates the importance of surface adsorbed hydrated proton species and highlights several key dynamic features of the solid-liquid interface, including proton confinement at the heterogeneous interface. Several methods were used for structural characterization before any calculations of the free energy are considered. These include radial pair distribution functions (g(r)), oxygen coordination shell numbers (CN), atomic density profiles, angular distribution functions and self-diffusion coefficients of water (D_0), all of which are key descriptors for heterogeneous interfaces[35]. For clarity, Pt(111) with H_2O molecules will be referred to as system A (defined as H_2O/Pt(111)), and Pt(111) with a proton in the presence of the H_2O molecules as system B (defined as H_3O^+/Pt(111)). Our results could greatly impact how we treat surface reactions at solid-liquid

interfaces and more importantly they could possess significant implications in electrochemistry and other related fields.

Computational Methods

All simulations were carried out using the Vienna Ab Initio Simulation Package (VASP)[36,37]. The Perdew−Burke−Ernzerhof (PBE) functional[38] was employed to describe exchange-correlation effects, the dispersion force correction was described using the Grimme D3 method[39] with Becke-Jonson damping[40] and a plane wave cut-off energy of 400 eV. The projected augmented wave method (PAW)[41,42] has been used. Atomic coordinates were relaxed under the conjugate gradient algorithm until the Hellmann-Feynman forces on all relaxed atoms fell below 0.05 eV/Å. The crystal structure of Pt(111) was optimised at the PBE-D3 level, yielding a lattice constant of 3.94 Å, which is in excellent agreement with previous theoretical[43,44] and experimental studies[45]. The canonical ensemble conditions were imposed by a Nose-Hoover thermostat[46] (NVT) for all the free energy calculations at 300 K. A 1.0 fs time step was used for molecular dynamics (MD) simulations, as it equates to approximately $1/10^{th}$ the timescale of the shortest mode commonly found in water molecules. The velocities were rescaled every 8 steps to readjust to the target temperature. The calculations used a 4 layer Pt(111) metal slab whereby for umbrella sampling calculations a 2 × 2 (16 Pt atoms) periodically repeated cell was used and a 2 x 4 (32 Pt atoms) supercell for all statistical analysis i.e. RDF (radial pair distribution function), coordination number and dipole orientation angle. The bottom two Pt layers were fixed to their corresponding bulk value.

The water slab consisted of either 11 or 22 water molecules placed on the Pt(111) surface to explicitly simulate the H_nO^x/Pt(111) interface with a fixed density of 1.0 $Kg{\cdot}m^{-3}$ and allowed to thermally equilibrated for a period of 5 ps before being subjected to a period of 50

ps for further analysis. The thickness of the water slab is 1.2 nm corresponding to ~3 layers of water, which is just within the experimental limit for detecting density fluctuations (~1.0 nm)[47]. All MD simulations used a 2x2x1 k-point integration of the Brillouin zone while static DFT calculations used a 6x6x1 k-point integration of the Brillouin zone.

The umbrella sampling (AIMD-US) calculations were carried out through biased molecular dynamics modules using the VASP code[48,49]. A Gaussian peak module of height -393.94 kJ mol^{-1} and width 48.24 kJ mol^{-1} were chosen to control the harmonic constraints. A set of multidimensional primitive coordinates were carefully selected which took the form of two collective variables (CV). The first was the conservation of the Pt-H distance along the reaction coordinate (CV1). The second was an angular constraint of 180º perpendicular to the Pt surface. This was controlled so that the angular variation was less than 10º. The simulations were carried out over a combined time scale of ~1200 ps. Free energy profiles were recovered with the weighted histogram analysis method (WHAM)[50,51]. On using US, the predicted free energy differences and free energy barriers explicitly include both solvent and entropy effects. It should be noted that the macroscopic behaviour of liquids can be imitated, but not exactly replicated using AIMD-US. Specifically, the problem arises due to finite size effects imposed by periodic boundary conditions, meaning we cannot reproduce the exact macroscopic structure of liquids. This is especially important for the water structure, which will exhibit an artificial order not commonly observed in the bulk liquid. However, for the purposes of this study, we are mainly interested in hydrogen transfer from the surface to the interfacial water layer, meaning our current model should give a reliable description of the solvation behaviour.

Furthermore, the effect of electric fields on the adsorption of covalently bonded species, such as H, on the surface relative to H_2O has been found to be negligible.[52] Whereas when closed shell molecules are considered, such as CO_2, the electric field has a considerable effect

on the adsorption behaviour[53]. The US process is schematically summarized in the SI section along with other calculation details used in the current work.

Results and Discussion

Structure of H_nO^x/Pt(111) Interface

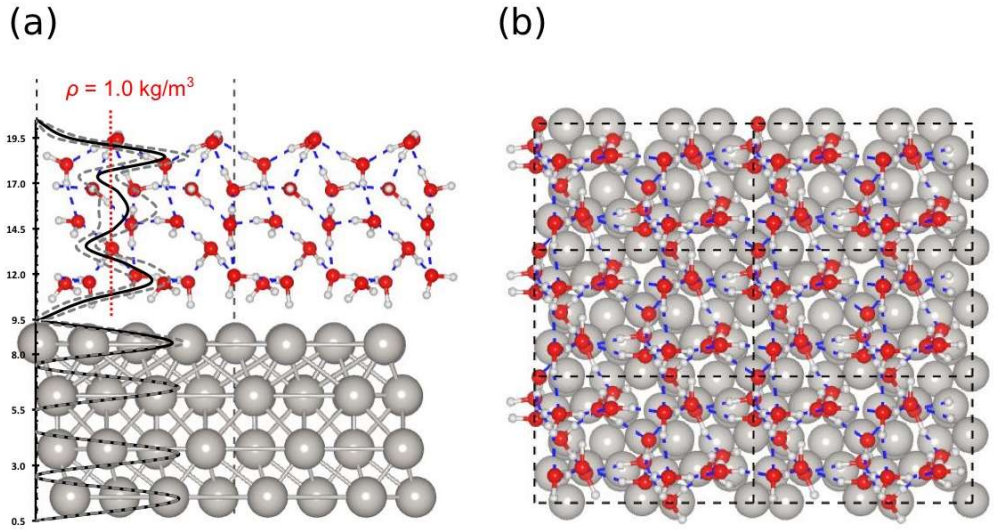

Figure 1. Snapshot of the simulation after 50 ps at the H_3O^+/Pt(111) interface from side view **(a)** and top view (2x3 periodically repeated supercell) **(b).** Approximately three layers of water can be distinguished based on the atomic density profile shown in panel (a). Here, the black line indicates the average atomic density, grey dashed lines indicate the min/max density flux throughout the duration of the simulation and the red line indicates the density of bulk water (1.0 $kg{\cdot}m^{-3}$).

The density profile shown in Figure 1(a) illustrates that our simulation contains ~3 water layers, with a thickness of 1.2 nm. Since the vast majority of reactions occur within the first two water layers, our model should give a reasonable description for understanding surface reactions. To adequately relax the hydrogen bond (HB) network at 300 K, a thermal equilibration period of 50 ps was performed, which is deemed necessary for structural analysis.

From our starting structure, we carried out calculations using a number of

characterization techniques which should give a solid foundation in the understanding of the interfacial structure and dynamics. The oxygen pair correlation function, $g_{o\text{-}o}(r)$, was computed, which provides quantitative information regarding the structure of the solvation shells of each water molecule and helps to characterise the differences in the water phases. For the purpose of clarity, in this study we only consider the first coordination shell of the water layer located at ~2.8 Å. Any variation in peak size or position would suggest that the H-bonding network has been distorted by the interface and/or the additional H.

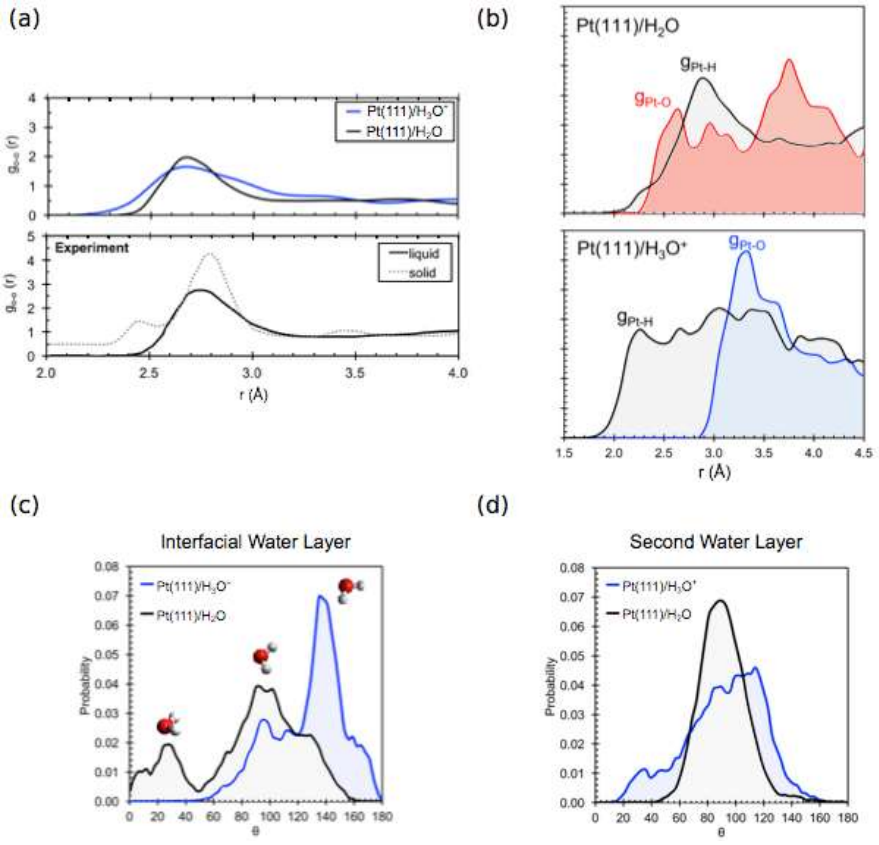

Figure 2. (a) Calculated oxygen-oxygen RDF $g_{O\text{-}O}(r)$ after 50 ps for both protonated (blue) and neutral (black) systems and experimentally[54] obtained data for liquid (water: 298K and 0.1 MPa, black line) and solid phase (ice: 122K, dashed grey line) water. **(b)** The radial pair distribution function (g(r)) for $g_{Pt\text{-}O}$ and $g_{Pt\text{-}H}$, calculated for both protonated (blue and grey) and neutral (red and grey) water systems. Dipole orientation angle distribution for neutral (grey) and protonated (blue) systems are calculated for **(c)** interfacial water layer and **(d)** second water layer (see SI for details).

147 A comparison between experimental and theoretically calculated $g_{O\text{-}O}(r)$ is shown in
148 Figure 2(a), from which we can confirm that we are indeed simulating a liquid-solid interface,
149 as the corresponding g(r) shows very few of the characteristics of ice and agrees quite well
150 with that of liquid water.

151 It is clear that system A (H_2O/Pt(111)) has a similar first coordination shell to that
152 reported by neutron diffraction studies for liquid water[54] ; despite having a slightly decreased
153 intensity, the separation distance r is the same. This suggests that the water coordination
154 environment has changed due to interactions with the Pt(111) surface, while the distance at
155 which O species are separated remains the same. Interestingly for system B (H_3O^+/Pt(111)),
156 the first peak shows a considerable broadening, a feature that is consistent with the existence
157 of structures of varying coordination number being formed.

158 More specifically, the peak broadening is a direct result of oxygen atoms restructuring
159 into a range of cationic species, like those depicted in Figure S2(b), as the excess proton is
160 transferred between water structures. This analysis agrees well with work by Bellarosa et al.[55]
161 on the H_2O/Ru(0001) interface, whereby a similar broadening of the first $g_{o\text{-}o}(r)$ peak was
162 observed as a result of water configurations formed to accommodate for the additional OH and
163 H species formed after water dissociation.

164 On integrating over the first g(r) peak, we can readily extract the coordination number
165 of the first coordination shell of oxygen, shown in Figure S2(a). Here, the excess H causes
166 fluctuations between co-ordinately saturated (CN > 4) and unsaturated (CN < 4) structures in
167 an effort to maintain a CN similar to that of bulk water, which is energetically more favourable.
168 For system B (H_3O^+/Pt(111)), a number of conjugated proton species are observed which
169 correspond to the cations found in other studies[56].

170 These findings are in good agreement with work by Kim et al.[57] who reported that H_3O^+
171 (hydronium) is absent from the platinum surface, with the proton preferentially existing in a

dynamic equilibrium of various multiple hydrated species of general formula: $H_{2n+1}O_n^+$. More specifically, the $H_5O_2^+$ (Zundel), $H_7O_3^+$ (planar Eigen) and $H_9O_4^+$ (Eigen) cations were observed most frequently at the interface. It is suggested that the high concentration of Zundel-like species at the interface, with its innate ability to interconvert between several two-dimensional analogues, make it ideally suited for proton transport at interfaces. From the g(r) and CN analysis, we have shed light on processes such as proton transfer and water restructuring that take place to accommodate for the additional H.

To further investigate the differences between the two systems, we calculated the dipole orientation distribution of the interfacial (0.0 Å−4.5 Å from surface) and second (4.5 Å−9.0 Å from surface) water layers; this analysis can be viewed as complimentary to g(r), as it permits for the determination of the preferred configuration of water within specific predefined regions. We find that the water molecules are arranged rather differently when comparing system A (H_2O/Pt(111)) with system B (H_3O^+/Pt(111)), with significant differences in the net dipole moment existing between the two systems. As can be seen from the distribution functions and dipole orientation analysis in Figure 2(c)-(d), the interfacial water layer of the neutral system sits <2.5 Å from the surface and displays a range of H-down and O-down configurations, which is consistent with previous studies[58]. For system B (H_3O^+/Pt(111)), the water layer is located <3.5 Å and adopts an almost exclusive H-down configuration at the interface attributed to the slight negative potential of the system when H is solvated. The configuration of the charged interfacial water layer is in accordance with that observed for the Ag(111)/H_2O electrified interface in previous work by M. Toney *et al.* [59, 60], giving further validation to our model.

The second water layer of system A (H_2O/Pt(111)) exhibits a normal distribution of its dipole angles centred at 90º. The result indicates a well-mixed second water layer that has little interaction with the interfacial water layer. Previous studies[61,62] have suggested that this feature is caused by a hydrophobic water layer existing directly above the Pt surface, through which

197 the interfacial water monolayer is ordered in such a way as to have few uncoordinated sites
198 available for hydrogen bonding with the subsequent water layers. System B (H_3O^+/Pt(111)),
199 on the other hand, shows a perturbation from a normal distribution, meaning that a weak
200 interaction with the interfacial water layer and Pt(111) surface exists.

201 To help justify our discussion and further explore the solvent-surface interactions, we
202 calculated the temperature dependant self-diffusion coefficients of water (D_0 (T)), the results
203 of which are summarised in Figure 3(a) (for methodology see SI for details). A stronger
204 interaction would result in a lower value of D_0 and vice versa for a weaker interaction. From
205 Figure 3(a), the general trend for D_0 at 300 K follows that bulk < system A < system B. This
206 can be rationalised by exploring the subtle differences between each system. For instance, the
207 influence of the Pt(111) surface in system A (H_2O/Pt(111)) results in a larger diffusion
208 coefficient when compared to that of bulk water, indicating that the interaction with the surface
209 is only slight. The combined influence of the Pt(111) surface and additional H in system B
210 (H_3O^+/Pt(111)) leads to the largest diffusion coefficient over all temperatures, being more than
211 doubled when compared to system A (H_2O/Pt(111)) and bulk water.

212 With the combination of these various structural characterization techniques, it
213 becomes apparent that the two systems are structurally and chemically very different. Despite
214 seeming trivial, the additional H causes profound differences in the ordering and therefore
215 dynamics of the water layers. It becomes evident that structural changes of the water layer
216 have significant influence on the dynamics and interaction of the water layer with the surface.

Surface Dynamics

(a)

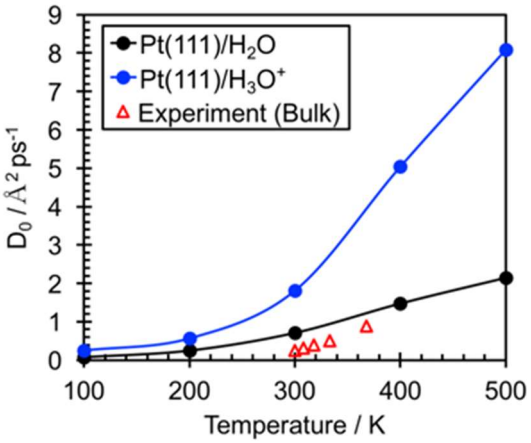

(b)

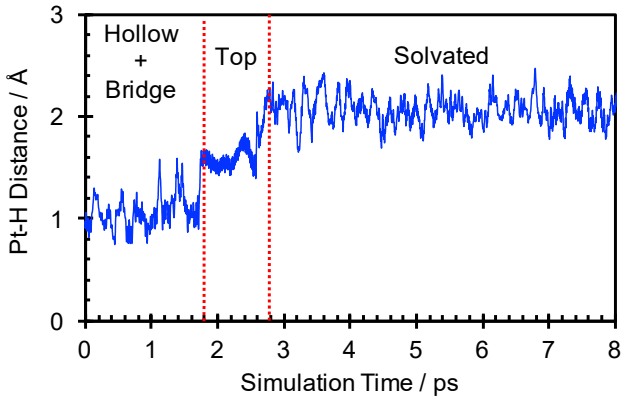

(c)

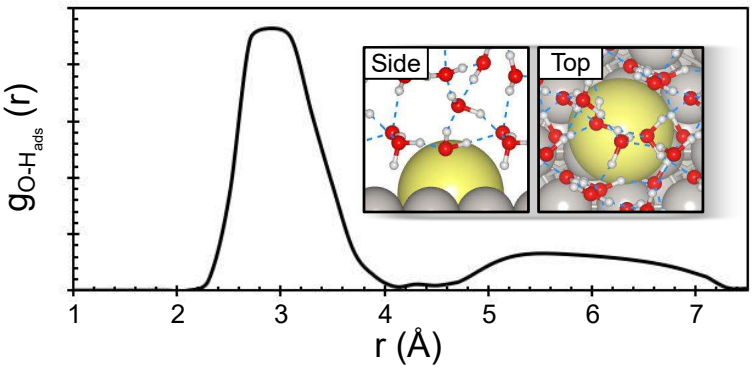

Figure 3. (a) Self-diffusion coefficients of water (D_0 (T)) (AIMD calculations: solid lines and circles). For comparison, experimental neutron scattering data[63] for bulk liquid water are also reported (red triangles). **(b)** Position of adsorbed hydrogen atom from the center of mass of Pt(111) surface over the course of an 8 ps free AIMD run. **(c)** Calculated RDF for the distance between the adsorbed hydrogen on Pt surface and oxygen atoms of the aqueous layer (note: $g_{O\text{-}H_{ads}}$ is averaged over all adsorbed sites on the Pt(111) surface). The sphere of repulsion exhibited by H_{ads} is represented in yellow.

Once adsorbed on the surface, hydrogen exhibits translational motion between the various sites of Pt(111) with relative ease. This process is highlighted by measuring the separation distance between H and the centre of mass of the top most Pt layer, over the course of a free MD simulation, shown in figure 3(b). In particular, H moves in a stepwise fashion between the various surface sites before desorbing from the top site into the solution after ~3 ps. Once in solution the protonated structures remain confined to the interface, and sit just above the surface with their preferential H-down geometry.

A pre-requisite for surface desorption is that H must be in close proximity to the water layer as to minimise the Pauli repulsion exhibited by the water molecules lone pair ($2a_1$, $3a_1$ and $1b_1$ orbitals) with the Pt d-band electrons. To facilitate this, charge transfer stabilization in the form of oxygen lone pair depopulation must occur, as well as a favourable dipole alignment of the water molecules and metal surface[64,65,66]. Desorption is, therefore, most likely to occur from the top site position where the repulsive interaction can be sterically minimised. In contrast, from the fcc hollow site, the H species lies closer to the centre of mass of the Pt(111) surface atoms; therefore, the Pauli repulsion is at its most prominent. The structuring of the water molecules facilitates adsorption/desorption at the top position, as the intermediate species align favourably, with water molecules preferentially existing above the Pt top site position.

On calculating the charge density difference (CDD) of H_{ads} (Figure S2(c), see SI for details) on the surface we see that electrons accumulate (green) just above the Pt surface. A clear change in the surface dipole moment is exhibited on adsorption of H from solution onto the surface. Here, H behaves akin to a negatively charged hydride with a small amount of negative charge density being accumulated in the vicinity of H_{ads} which exhibits a sphere of repulsion between itself and the nearest neighbouring closed shell water molecules. The radius of the sphere is calculated to be ~2.95 Å (Figure 3(c)), a distance which is surprisingly non-site specific. That is to say, the sphere of repulsion is maintained regardless of the adsorbed

site, which can be attributed to a number of phenomena: the interaction of H_{ads} with the lone pair of water[67] and the change in the dipole moment of Pt(111) surface relative to the water molecules. This means that the system must be given sufficient simulation time so that the water molecules can rearrange to allow for a favourable dipole interaction.

It should be noted that the general phenomena of water layer repulsion by adsorbed species has been reported previously[68]. Of particular interest is the work by Roman and Groß[69] for the case of a fully saturated Pt(111) surface by H, which similar to the present study, they showed how the water layer is repelled by an additional 1 Å above the Pt(111) surface, when compared to the clean surface. However, we find that even a single adsorbed species can causes weakening of the interaction of the water layer with the Pt(111) surface. We suggest that it is the accumulation of additional adsorbed hydrogen species which allows for stable areas of hydrogen adsorbed on the surface under electrochemical conditions.

The interaction between the solvent and substrate coupled with proton confinement at the interface give an insight into the efficiency of hydrogen transfer on Pt(111), whereby we observe global structure changes of the water layer at each stage of the reaction, even proceeding adsorption. The effects of H confinement at the interface as solvated cation species, on the other hand, make for ideal hydrogen transfer vessels to and from the surface top site.

Free Energy Landscape

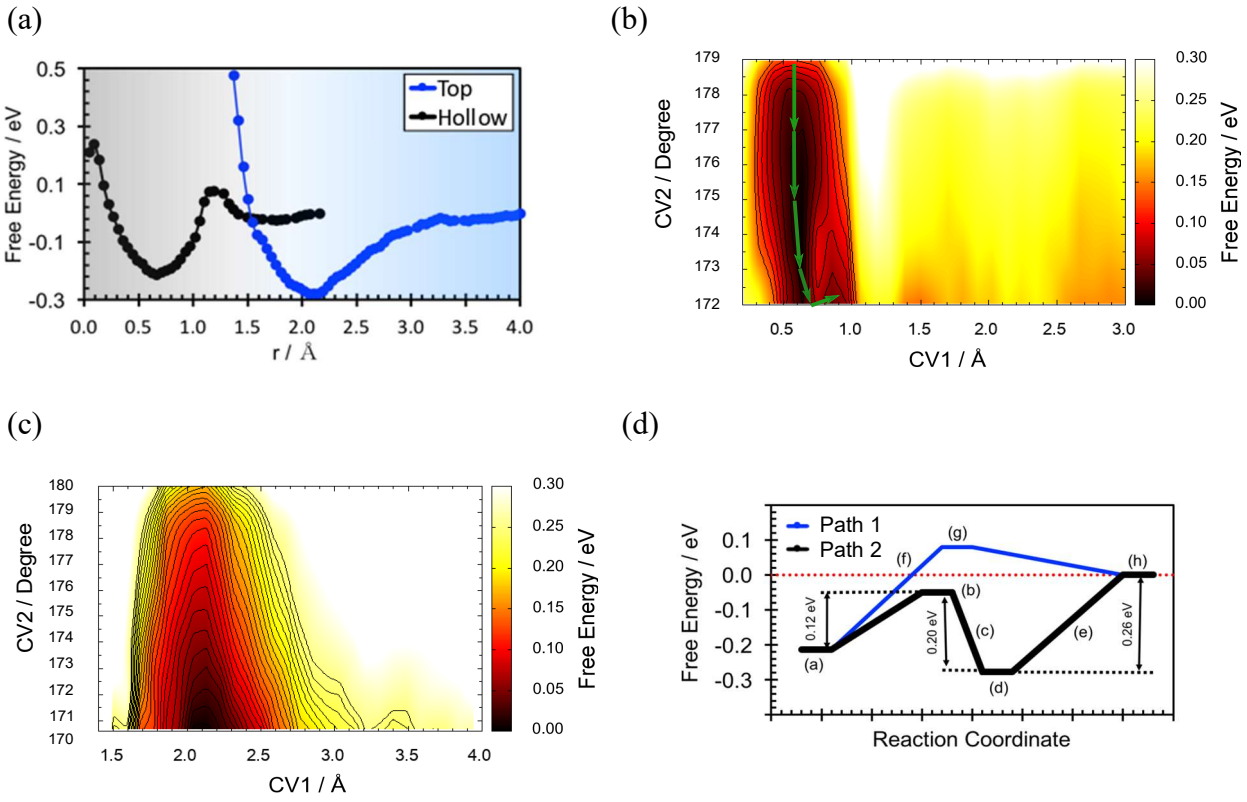

Figure 4. The average free energy profile for adsorption/desorption from each site is shown in panel **(a)** 2D free energy profile for proton adsorption/desorption as a function of two collective variables – distance from the Pt surface (CV1) and the angle orthonormal to the surface layer (CV2) from; **(b)** the fcc-Hollow site (green arrows highlight our proposed MEP); and **(c)** Top site. To achieve adequate sampling and thermodynamic equilibration, each sample was taken at intervals of 0.05 Å and each constrained simulation was carried out for between 8 and 30 ps. (For clarity, black contour lines are set to intervals of 0.03 eV). **(d)** The relative free energy for steps involved in pathway 1 (blue) and 2 (black), derived from AIMD umbrella sampling calculations. The reaction steps correspond to those shown in Figure 5.

To determine the lowest energy pathway for hydrogen adsorption/desorption, finally and perhaps more importantly we calculated the free energy landscape from the fcc-hollow and top sites, respectively. These calculations include the effects of direct solvation and the formation of hydrogen bonds between surface species and water molecules (See SI, for details). The free energy profiles for hydrogen adsorption/desorption are summarised in Figure 4(a)-(d).

Starting from H_{ads} at the hollow and top sites, we applied harmonic constraints (for details see SI) to acquire the population along the Pt-H collective variable, driving H to solvate into the bulk solution. As can be seen from Figures 4(b) and 4(c), the free energy along the hollow site trajectory is highly angular dependant; a decrease in the desorption barrier with decreasing angle is observed. In other words, H favours moving to the neighbouring bridge site rather than direct solvation, which suggests that diffusion to various sites on the surface occurs with ease and with small free energy barriers calculated to be less than 0.12 eV.

Surprisingly, from Figure 5(a)-5(c), we find that H adsorbed on the top site is spontaneously solvated by two surface water molecules, whereby H on the top site proves to be only quasi-stable, a fact which is reflected in its short lifetime (~2-8 ps), before being quickly solvated. From this we infer that the most stable state for hydrogen is in the form of a surface adsorbed hydrated proton, which bridges two top site positions and is located ~2.1 Å from the Pt surface, as shown in Figure 5(d). The stability of these structures is further explored on taking CDD profiles for the interaction of the hydrated protons and the Pt(111) surface, provided in SI. The significant charge overlap at the interfacial region coupled with the local minimum in the free energy profile indicates that these species are indeed stable and exist as chemisorbed cations rather than as free protons. This finding is consistent with recent work by Kim et al.[70] who reported, using mass spectrometry and refection adsorption infrared spectroscopy, that adsorbed hydrogen species ionize into stable multiple hydrated protons on the surface.

Snapshots from the sampled trajectories are shown in Figure 5, which have been selected under the guidance of calculated free energy values (Figure 5). Figure 5(d) represents the lowest energy pathway for H desorption from the Pt(111) surface to the aqueous solution. Our calculations show that pathway 2 (desorption from the hollow-bridge-top site and then on

to the water layers) is more favourable when compared to pathway 1 (direct hollow site desorption) in the realm of free energy.

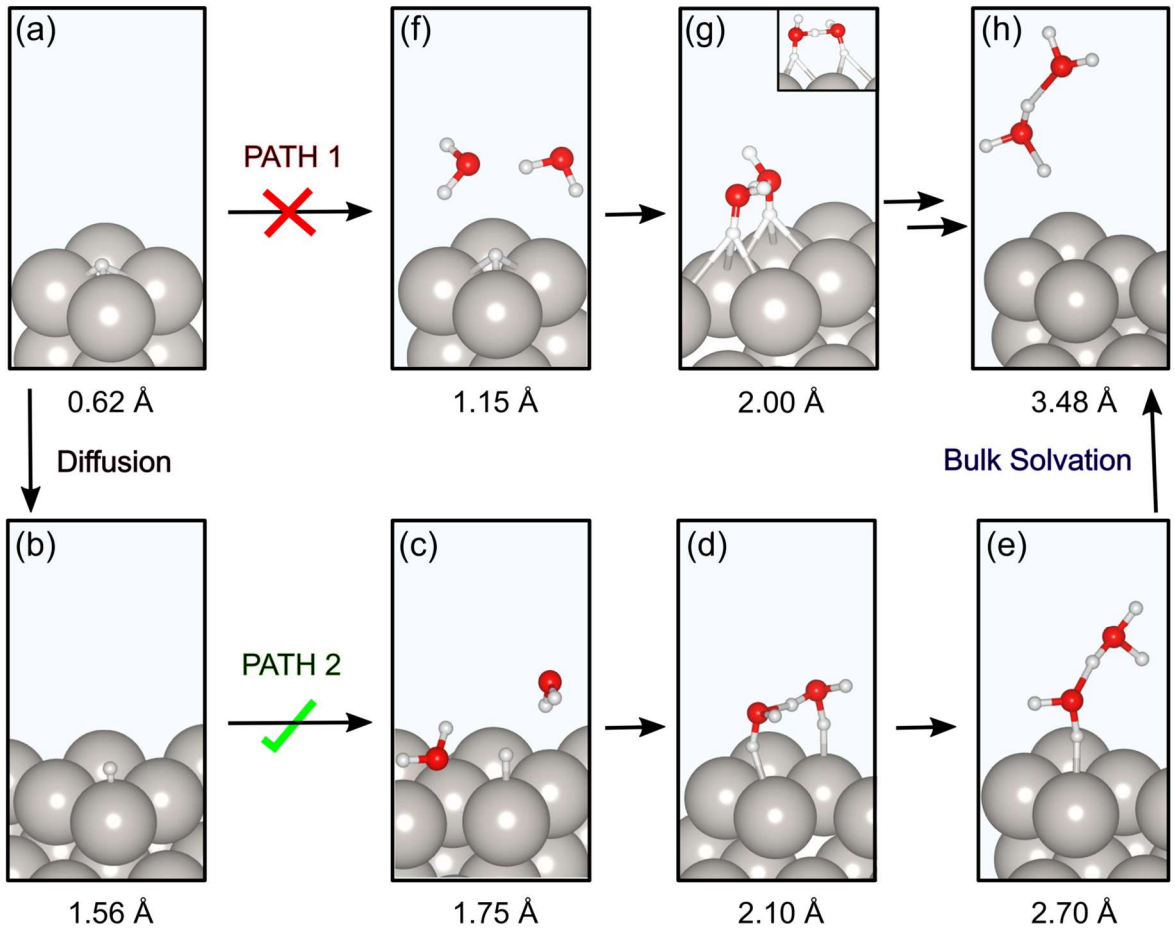

Figure 5. Several snapshots of our proposed pathway for hydrogen transfer from the surface to the solution obtained from constrained AIMD simulations. Path 1 shows process of direct desorption via the Hollow site while Path 2 shows our proposed desorption pathway via diffusion from hollow-bridge-top sites.

From the results above, we can see that the reaction occurs as follows; firstly, due to the low barrier associated with hydrogen migration ($\Delta G^{\ddagger}$ = 0.12 eV), if hydrogen is adsorbed on the hollow site, it can move via the bridge site to the top site (Figures 5(a)-(b)). It should be noted that as the coverage increases to the experimental value of ~0.66 ML[28] the barrier for H migration will increase. The free energy for the formation of cations above the top site is

energetically favourable ($\Delta G^{\ddagger}$ = -0.23 eV) and will therefore form spontaneously, here the proton preferentially exists 2.1 Å above the top site position, as shown in Figure 5(d). At low H coverages, it becomes unfavourable for the proton at the interface to transfer to subsequent water layers (confinement), as shown in Figure 5(h), with a barrier of 0.26 eV required for further solvation into the bulk solution. This leads to a stable protonated water structures that are confined to the interface with predominantly H-down geometry. The presence of these surface adsorbed cations could enhance hydrogen transfer to and from the surface, leading to significant mechanistic consequences for HER, water splitting and other catalytic reactions involving hydrogen transfer.

From previous studies, the H atom potential energy surface (PES) for transition metals along the (111) crystallographic axis is quite flat[71]. Therefore, we believe that our findings for Pt(111) are of general importance. However, we acknowledge that a specific study exploring the physical origin of different catalytic behaviors, of the same chemical composition, but on different crystal phases and/or surfaces is highly desirable.

Conclusion

In this work, we have performed enhanced AIMD sampling methodologies and DFT calculations to study the structure and reactivity of H_nO^x/Pt(111) interface. We have attempted to obtain an atomistic picture of how the aqueous medium effects the structure and reactivity of the solid-liquid interface. Based on our calculations and analyses, the following conclusions can be drawn:

1. The addition of H to H_2O/Pt(111) results in a profound difference in the structure of the interfacial water layer. We find that the strength of the solid-liquid interaction and the configuration of water molecules above the reaction site are of key importance.

2. We exemplify the specific reaction conditions required for H transfer to occur. The lifetime of adsorbed hydrogen on Pt(111) is short lived at low coverage and preferentially exist as a confined cation structure at the interfacial region.

3. The free energy landscape for hydrogen transfer at the H_2O/Pt(111) interface is obtained and a reaction pathway for the Volmer reaction is proposed, which includes surface adsorbed hydrated protons as key intermediates. The importance of top site adsorbed cations as key reaction intermediates for hydrogen transfer on Pt(111) is emphasized.

Acknowledgements

P.H, C.G, Y.M and P.S.R all acknowledge the use of computational resources from the U.K national high-performance computing service, ARCHER, for which access was obtained via the UKCP consortium. P.S.R thanks his PhD studentship funded by the Northern Ireland Department for the Economy (NI-DfE) at the Queen's University of Belfast.

References

(1) M. S. Dresselhaus and I. L. Thomas, *Nature*, 2001, **414**, 332−337.

(2) S. Shafiee and E. Topal, *Energy Policy*, 2009, **37**, 181−189.

(3) M. Z. Zarobson, W. G. Colella and D. M. Golden, *Science*, 2005, **368**, 1901−1905.

(4) R. Dufo-Lopez and J. L. Bernal-Agustin, *Renew. Energy*, 2008, **33(12),** 2559−2572.

(5) R. C. Alkire, D. M. Kolb, J. Lipkowski and P. N. Ross , Advances in electrochemical science and engineering vol. 9, Wiley-VCH, Weinheim, 2006.

(6) T. Fukuma. *Sci. Technol. Adv. Mater*., 2010, **11**, 033003.

(7) M. Watkins, M. L. Berkowitz and A. L. Shluger. *Phys. Chem. Chem. Phys.*, 2011, **13**, 12584−12594.

(8) S. Yamamoto, H. Bluhm, K. Andersson, G. Ketteler, H. Ogasawara, M. Salmeron and A. Nilsson, *J. Phys. Condens. Matter*, 2008, **20**, 184025.

(9) N. Agmon, *Chem. Phys. Lett.*, 1995, **244**, 456.

(10) W. Schmickler and E. Santos, Interfacial Electrochemistry (Oxford Univ. Press, New York, 1996).

(11) D. van der Vliet, D. S. Strmcnik, C. Wang, V. R. Stamenkovic, N. M. Markovic and M. T. M. Koper, *J. Electroanal. Chem.,* 2010, **647**, 29−34.

(12) J. Carrasco, A. Hodgson and A. Michaelides, *Nat. Mater.,* 2012, **11**, 667–674.

(13) J. Peng, D. Cao, Z. He, J. Guo, P. Hapala, R. Ma, B. Cheng, J. Cheng, W. J. Xie, X. -Z. Li, P. Jelinek, L. -M. Xu, Y. Q. Gao, E. -G. Wang and Y. Jiang, *Nature*. 2018, **557**, 701.

(14) P. Ferrin, S. Kandoi, A. U. Nilekar and M. Mavrikakis, *Surf. Sci.,* 2012, **606**, 679−689.

(15) M. P. Hyman and J. W. Medlin, *J. Phys. Chem. B.,* 2006, **110**, 15338–15344.

(16) M. J. Janik, C. D. Taylor and M. Neurock, *J. Electrochem. Soc.*, 2009, **156**, B126–B135.

(17) T. Sheng, W-F. Lin, C.Hardacre and P. Hu, *J. Phys. Chem. C*., 2014, **118**, 5762–5772.

(18) S. Sakong, M. Naderian, K. Matthew, R. G. Hennig and A. Gross, *J. Chem. Phys*,. 2015, **142**, 234107.

(19) T. Cheng, H. Xiao and W. A. Goddard, *Proc. Natl. Acad. Sci. U.S.A.* 2017, **114**, 1795–1800.

(20) D. Wang, T. Sheng, J. Chen, H-F. Wang and P. Hu, *Nat. Catal.*, 2018, **1**, 291–299.

(21) Y. Sha, T. H. Yu, Y. Liu, B. V. Merinov and W. A. Goddard, *J. Phys. Chem. Lett*. 2010, **1**, 856–861.

(22) Y-H. Fang, G-F. Wei and Z-P. Liu, *J. Phys. Chem. C.,* 2014, **118***,* 3629–3635.

(23) Y-H. Fang and Z-P. Liu, *ACS Catal.*, 2014, **4**, 4364–4376.

(24) S. Schnur and A. Groß, *New J. Phys.,* 2009, **11**, 125003.

(25) J. P. Guthrie, *J. Am. Chem. Soc.,* 1996, **118**, 12886.

(26) P. J. Feibelman, *Science,* 2002, **295**, 99–102.

(27) A. Michaelides, *Appl. Phys. A.*, 2006, **85**, 415.

(28) S. Schnur and A. Groß, Catal. Today, 2011, **165**, 129–137.

(29) N. M. Markovic, B. N. Grgur and P. N. Ross, J. Phys. Chem. B., 1997, **101**, 5405.

(30) A. Michaelides and P. Hu, *J. Am. Chem. Soc.* 2001, **123**, 4235−4242.

(31) K. Kunimatsu, T. Senzaki, M. Tsushima and M. A. Osawa, *Chem. Phys. Lett.*, 2005, **401**, 451.

(32) E. Skulason, G. S. Karlberg, J. Rossmeisl, T. Bligaard, J. Greeley, H. Jonsson and J. K. Nørskov, *Phys. Chem. Chem. Phys.,* 2007, **9**, 3241.

(33) E. Skulason, V. Tripkovic, M. E. Bjorketurn, S. Gudmundsdottir, G. Karlberg, J. Rossmeisl, T. Bligaard, H. Jonsson and J. K. Nørskov, *J.* Phys. Chem. C*.,* 2010, **114**, 18182–18197.

(34) C. Guo, Z, Wang, D. Wang, H. -F. Wang and P. Hu, *J. Phys. Chem. C*, 2018, **122**, 21478−21483.

(35) A. K. Soper and M. A. Ricci, *Phys. Rev. Lett.*, 2000, **84**, 2881.

(36) G. Kresse and J. Hafner, *Phys. Rev. B.*, 1993, **48**, 13115−13118.

(37) G. Kresse and J. Furthmüller, *Phys. Rev. B.*, 1996, **54**, 11169−11186.

(38) J. P. Perdew, K. Burke and M. Ernzerhof, *Phys. Rev. Lett.,* 1996, **77**, 3865−3868.

(39) S. Grimme, J. Antony, S. Ehrlich and H. Krieg, *J. Chem. Phys.*, 2010, **132**, 154104.

(40) S. Grimme, S. Ehrlich and L. Goerigk, *J. Comp. Chem.,* 2011, **32**, 1456.

(41) P. E. Blochl, *Phys. Rev. B: Condens. Matter Mater. Phys., 1994,* **50**, 17953−17979.

(42) G. Kresse and D. Joubert, *Phys. Rev. B: Condens. Matter Mater. Phys.,* 1999, **59**, 1758−1775.

(43) J. Carrasco, J. Klimes and A. Michaelides, *J. Chem. Phys.*, 2013, **138**, 024708.

(44) I. Hamada, K. Lee and Y. Morikawa, *Phys. Rev. A.*, 2010, **81**, 115452.

(45) H.B. Michaelson, *J. Appl. Phys.*, 1977. **48**, 4729.

(46) W. G. Hoover, *Phys. Rev. A.,* 1985, **31**, 1695.

(47) C. Huang, K. T. Wikfeldt, T. Tokushima, D. Nordlund, Y. Harada, U. Bergmann, M. Niebuhr, T. M. Weiss, Y. Horikawa, M. Leetmaa, M. P. Ljungberg, O. Takahashi, A. Lenz, L. Ojamae, A. P. Lyubartsev, S. Shin, L. G. M. Pettersson, and A. Nilsson, *Proc. Natl. Acad. Sci. U. S. A.*, 2009, **106**, 15214−15218.

(48) G. M. Torrie and J. P. Valleau, *J. Comp. Phys.,* 1997, **23**, 187.

(49) D. Frenkel and B. Smit, Understanding molecular simulations: from algorithms to applications (Academic Press: San Diego, 2002).

(50) S. Kumar, D. Bouzida, R. H. Swendsen, P. A. Kollman and J. M Rosenberg, *J. Comput. Chem.,* 1992, **13**, 1011–1021.

(51) S. Kumar, J. M. Rosenberg, D. Bouzida, R. H. Swendsen and P. A. Kollman, *J. Comput. Chem.* 1995, **16**, 1339−1350.

(52) J. Rossmeisl, J. K. Nørskov, C. Taylor, M. Janik, and M. Neurock, *J. Phys. Chem. B.*, 2006, **110**, 21833.

(53) S. Gudmundsdóttir, W. Tang, G. Henkelman, H. Jónsson and E. Skúlason, E. *J. Chem. Phys.*, 2012, **137***,* 164705.

(54) A. K. Soper, *Chem. Phys.* 2010, **258**, 121−137.

(55) L. Bellarosa, R. Garcia-Muelas, G. Revilla-Lopez and N. Lopez, *ACS Cent. Sci.,* 2016, **2**, 109−116.

(56) P. Quaino, N. B. Luque, G. Soldano, R. Nazmutdinov, E. Santos, T. Roman, A. Lundin, A. Gross and W. Schmickler, *Electrochim. Acta.* 2013, **105**, 248–253.

(57) Y. Kim, S. Shin and H. Kang, *Angew. Chem. Int. Ed.* 2015, **54**, 7626−7630.

(58) J. Le, A. Cuesta and J. Cheng, *J. Electroanal. Chem.,* 2017, **819**, 87−94.

(59) M. F. Toney, J. N. Howard, J. Richer, G. L. Borges, J. G. Gordon, O. R. Melroy, D. G. Wiesler, D. Yee and L. B. Sorensen, *Nature*, 1994, **368**, 444–446.

(60) M. F. Toney, J. N. Howard, J. Richer, G. L. Borges, J. G. Gordon, O. R. Melroy, D. G. Wiesler, D. Yee and L. B. Sorensen. *Surf. Sci.* 1995, **335**, 326–332.

(61) C. Wang, H. Lu, Z. Wang, P. Xiu, B. Zhou, G. Zuo, R. Wan, J. Hu and H. Fang, *Phys. Rev. Lett.,* 2009, **103**, 137801.

(62) D. T. Limmer, A. P. Willard, P. Madden and D. Chandler, *Proc. Natl. Acad. Sci. U. S. A.,* 2013, **110**, 4200–4205.

(63) F. G. Sanchez, F. Juranyi, T. Gimmi, L. Van Loon, T. Unruh and L. W. Diamond, *J. Chem. Phys.* 2008, **129**, 174706.

(64) T. Schiros, L. .-Å. Näslund, K. Andersson, J. Gyllenpalm, G. S. Karlberg, M. Odelius, H. Ogasawara, L. G. M. Pettersson and A. Nilsson, *J. Phys. Chem. C.,* 2007, **41**, 15003–15012.

(65) A. Michaelides, V. A. Ranea, P. L. de Andres, and D. A. King, *Phys. Rev. Lett.* 2003 **90**, 216102 (2003).

(66) M. T. Koper and R. A. van Santen, *J. Electroanal. Chem*. 1999, **472**, 126–136.

(67) I. Hamada and Y. Morikawa, *J. Chem. Phys.* 2011, **134**, 154701.

(68) M. Otani, I. Hamada, O. Sugino, Y. Morikawa, Y. Okamoto and T. Ikeshoji, *J. Phys. Soc. Jpn.,* 2008, **77**, 024802.

(69) T. Romana and A. Gross, *Catal. Today*, 2013, **202**, 183–190.

(70) Y. Kim, C. Noh, Y. Jung and H. Kang, *Chem. Eur. J.,* 2017, **23**, 17566–17575.

(71) G. Kallen and G. Wahnström, *Phys. Rev. B.,* 2001, **65**, 033406.